Interaction Notes

Note 231

May 1975

Limitations of Wire-Grid Modeling of a Closed Surface

K. S. H. Lee and Lennart Marin

The Dikewood Corporation, Westwood Research Branch
Los Angeles, California

and

J. P. Castillo

Air Force Weapons Laboratory
Albuquerque, New Mexico

Abstract

Three different approaches are used to discuss the differences between the current and charge densities calculated for a perfectly conducting closed surface and those for the wire grid that models the closed surface.

SECTION I

INTRODUCTION

Recently, the question has been raised regarding the validity of using the wire-grid model of a structure with a closed surface in EMP interaction calculations [1]. By EMP interaction calculations we mean calculations of current and charge densities induced on the closed surface of a structure. To be sure, the wire-grid model has certain attractive features from the viewpoint of computer programming and is capable of giving reliable far-field results, such as the radar cross section and the extinction coefficient of a scatterer. On the other hand, it is clear on physical grounds that the wire grid is a poor model of a closed surface for interaction calculations. Without loss of generality, let the closed surface of the actual structure and the wires of the wire-grid model be perfectly conducting (Figs. 1a and 1b). Then, the former has an interior region where the field vanishes identically, whereas the latter has an evanescent reactive field hugging both sides of the grid. Evidently, this means that the current and charge densities induced on the external surface of the actual structure must differ from the corresponding "averaged" quantities on the outer side of the grid when both structures are immersed in the same incident wave. The differences will be quantified in the following three sections, each of which is based on an approach of its own.

In Section II we employ certain spatial averaging on the $\underline{E}$-field integral equation appropriate for the wire-grid model of an actual solid structure and arrive at a perturbed integral operator valid on the closed surface of the actual structure. The standard first-order perturbation theory is then invoked to calculate the impedances that need to be subtracted from the wire-grid model so as to approximate the actual structure more closely. The special case of a solid sphere and the corresponding wire-grid sphere is treated as an example of the general theory. The impedances that need to be subtracted from the wire-grid sphere are given explicitly and the lowest natural frequencies are contrasted with those of the solid sphere. It is found that the wire-grid sphere (or, perhaps, the wire-grid model of a general-shaped body) has larger resonance frequencies and smaller damping constants than does the corresponding solid sphere.

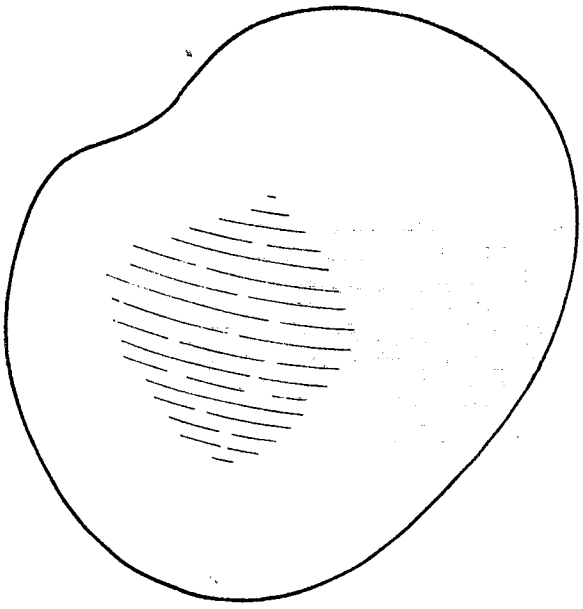

Fig. 1a. Perfectly conducting closed surface.

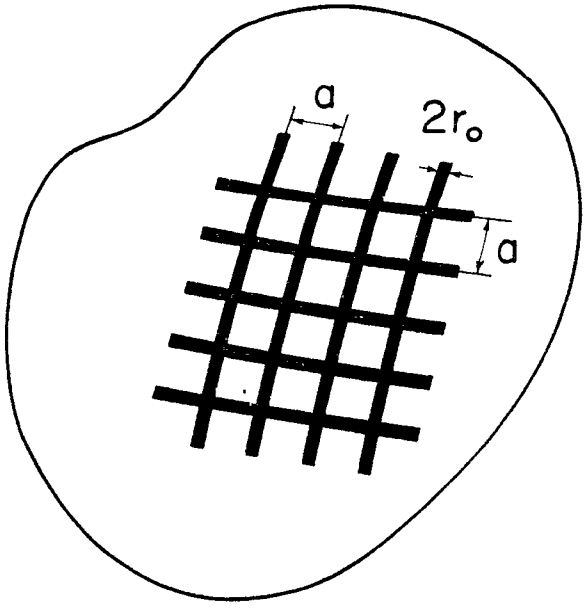

Fig. 1b. Wire-grid model of Fig. 1a.

In Section III we calculate the matrix elements from the E-field integral equation for the wire-grid model and for the corresponding structure with a closed surface. The comparison of the calculations shows that the diagonal matrix elements and the off-diagonal elements resulting from interactions between immediate neighboring patches are substantially smaller than the corresponding ones in the wire-grid model. The interactions between more distant patches, however, agree well with the interactions between corresponding wire segments. The calculations not only confirm one of the results in Section II that the induced currents are underestimated in the wire-grid model but also point to a way of correcting the matrix elements in computer codes based on the wire-grid model.

The matrix equation of the E-field integral equation that is commonly used in numerical computation can be interpreted as an N-port network. A different network representation is given in Section IV based on one of the many different forms of the E-field equation. This representation can be viewed as a "two-dimensional" transmission line and is more accurate for the wire-grid model. The network elements are calculated for the closed surface as well as for the corresponding wire-grid model.

SECTION II

FORMAL APPROACH

We begin with the so-called $\underline{E}$-field integral equation on the wire surface of Fig. 1b

$$\underline{\underline{\mathcal{L}}} \cdot \underline{J} = -\underline{E}^{inc}_{tan} \tag{1}$$

with

$$\underline{\underline{\mathcal{L}}} \cdot \underline{J} \equiv \underline{E}^{ind} + \underline{E}^{cap}$$

$$\equiv s\mu\, \hat{n}\times\hat{n}\times \int G(\underline{r},\underline{r}')\underline{J}(\underline{r}')dS' - \frac{1}{s\varepsilon}\, \hat{n}\times\hat{n}\times\nabla\nabla\cdot \int G(\underline{r},\underline{r}')\underline{J}(\underline{r}')dS' \tag{2}$$

where $\underline{E}^{ind}$ and $\underline{E}^{cap}$ can be interpreted respectively as the inductive and capacitive parts of the scattered field, $\underline{r}$ and $\underline{r}'$ belong to the wire surface, $\hat{n}$ is the outward unit normal, $\hat{n}\times\hat{n}\times \equiv (\hat{n}\hat{n} - \underline{\underline{I}})\cdot$, $\underline{\underline{I}}$ = unit dyad, $s = j\omega$ for time convention $e^{j\omega t}$. Note that $\underline{\underline{\mathcal{L}}}$ is a symmetric operator. For the moment, let us assume that after some spatial averaging of (1), e.g., integrating over a square cell in Fig. 1b, we have, on the closed surface of the structure (Fig. 1a),

$$(\underline{\underline{\mathcal{L}}}_o - \underline{\underline{\mathcal{L}}}')\cdot\underline{K} = -\underline{E}^{inc}_{tan} \tag{3}$$

where $\underline{\underline{\mathcal{L}}}'$ is an impedance operator and considered to be a perturbation on $\underline{\underline{\mathcal{L}}}_o$, which is given by (2) when $\underline{r}$ and $\underline{r}'$ belong to the closed surface. When $\underline{\underline{\mathcal{L}}}'$ is zero, (3) becomes the $\underline{E}$-field integral equation on the closed surface of a perfectly conducting structure (Fig. 1a). For the perturbed operator $\underline{\underline{\mathcal{L}}}'$ we take, from [2],

$$\underline{\underline{\mathcal{L}}}' = \frac{s\mu a}{2\pi}\, \ell n\left(\frac{a}{2\pi r_o}\right)\left(\underline{\underline{I}} - \frac{c^2}{2s^2}\nabla_s\nabla_s\right) \tag{4}$$

Here, ∇_s is the surface gradient operator, a the length of wire segment,

r_o the wire radius (Fig. 1b), and $c^2 = (\mu\varepsilon)^{-1}$.

Let $\underline{J}_\beta$ and $\underline{K}_\beta$ be the normalized eigenvectors that diagonalize respectively the operators $\underline{\underline{\mathcal{L}}}_o$ and $\underline{\underline{\mathcal{L}}}_o - \underline{\underline{\mathcal{L}}}'$, i.e.,

$$\underline{\underline{\mathcal{L}}}_o \cdot \underline{J}_\beta = \lambda_\beta^o(s)\underline{J}_\beta \tag{5}$$

$$(\underline{\underline{\mathcal{L}}}_o - \underline{\underline{\mathcal{L}}}') \cdot \underline{K}_\beta = \lambda_\beta(s)\underline{K}_\beta \tag{6}$$

Applying the first-order perturbation theory to (6) we obtain [3]

$$\lambda_\beta(s) = \lambda_\beta^o(s) - L'_{\beta\beta}(s) \tag{7}$$

$$L'_{\beta\beta} = \int \underline{J}_\beta \cdot \underline{\underline{\mathcal{L}}}' \cdot \underline{J}_\beta \, dS \tag{8}$$

with

$$\int \underline{J}_\beta \cdot \underline{J}_\beta \, dS = 1$$

Let $s_{\beta,\beta'}$ and $s^o_{\beta,\beta'}$ be the zeros of λ_β and λ^o_β respectively. Then (7) gives approximately

$$s_{\beta,\beta'} \simeq s^o_{\beta,\beta'} + L'_{\beta\beta}(s^o_{\beta,\beta'}) \left[\frac{d\lambda^o_\beta}{ds}\right]^{-1}_{s^o_{\beta,\beta'}} \tag{9}$$

As an example, let us work out the case of a perfectly conducting sphere and the corresponding wire-grid model. We will calculate the natural modes, the eigenvalues (which are equal to the negatives of the eigenimpedances introduced in [4]), and the natural frequencies only for the lowest electric and magnetic modes of the wire-grid model and compare them with the corresponding ones of the solid sphere. From [5] we have, for a solid sphere of radius R, the following:

Table I. Solid Sphere

electric dipole mode	magnetic dipole mode
$\lambda_1^{o'}(s) = Z_o\left[\frac{sR}{c}\, i_1\left(\frac{sR}{c}\right)\right]'\left[\frac{sR}{c}\, k_1\left(\frac{sR}{c}\right)\right]'$	$\lambda_1^{o''}(s) = Z_o\left[\frac{sR}{c}\, i_1\left(\frac{sR}{c}\right)\right]\left[\frac{sR}{c}\, k_1\left(\frac{sR}{c}\right)\right]$
$\underline{J}_1' = \hat{\theta}\, \sin\theta$	$\underline{J}_1'' = \hat{\phi}\, \sin\theta$
$s_{1,\pm1}^{o'} = \left(-\frac{1}{2} \pm \frac{i\sqrt{3}}{2}\right)\frac{c}{R}$	$s_{1,0}^{o''} = -\frac{c}{R}$

where $Z_o = \sqrt{\mu/\varepsilon}$, $i_1(x)$ and $k_1(x)$ are the modified spherical Bessel functions, and the prime on the square brackets means differentiation with respect to sR/c.

We first evaluate L_{11}' and $(d/ds)\lambda_1^o$ with the above data for a solid sphere. Then we use (9) to calculate the corresponding natural frequencies of the wire-grid model. We find

$$s_{1,\pm1}' = -\frac{1}{2}\frac{c}{R}(1-\delta) \pm \frac{i\sqrt{3}}{2}\frac{c}{R}(1+\delta) \quad \text{(electric dipole mode)}$$

$$s_{1,0}'' = -\frac{c}{R}(1-\delta) \quad \text{(magnetic dipole mode)} \qquad (10)$$

$$\delta \equiv \frac{a}{2\pi R}\, \ell n\left(\frac{a}{2\pi r_o}\right)$$

In Fig. 2 we show the poles based on the above calculations and it can be seen that the wire grid has a higher Q value than the corresponding closed structure, as one might have expected intuitively.

It is interesting to point out that the eigenvectors $\underline{K}_{\ell m}'(\theta,\phi)$ and $\underline{K}_{\ell m}''(\theta,\phi)$ of a sphere defined in [6] diagonalize not only the operator $\underline{\underline{\mathcal{L}}}_o$ but also the perturbed operator $\underline{\underline{\mathcal{L}}}'$, i.e.,

$$\underline{\underline{\mathcal{L}}}' \cdot \underline{K}_{\ell m}' = s\mu R\delta\left[1 + \frac{c^2}{2s^2R^2}\,\ell(\ell+1)\right]\underline{K}_{\ell m}'$$

$$\underline{\underline{\mathcal{L}}}' \cdot \underline{K}_{\ell m}'' = s\mu R\delta\, \underline{K}_{\ell m}'' \qquad (11)$$

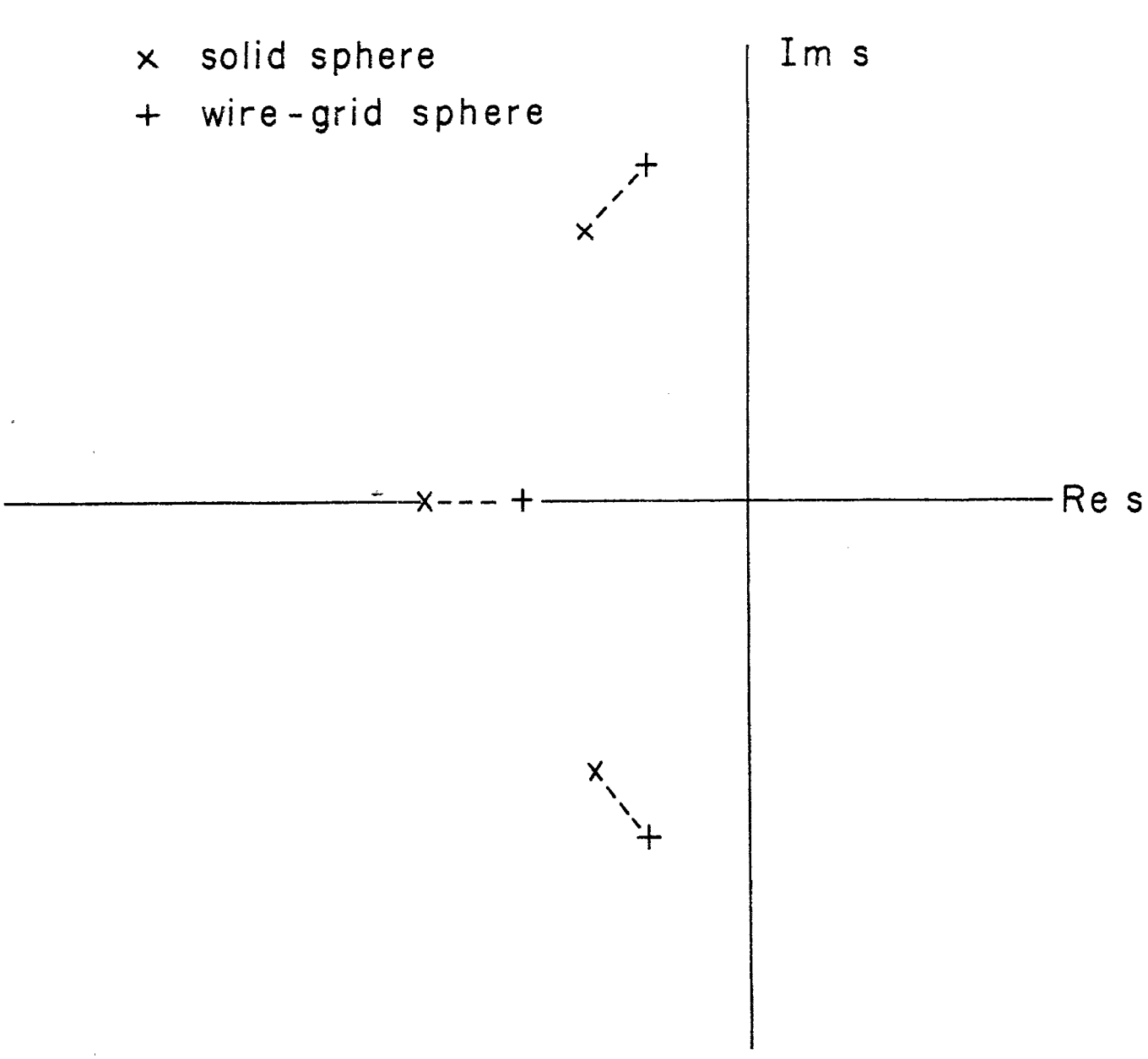

Fig. 2. Natural frequencies of electric and magnetic modes of a solid sphere and its wire-grid model.

The employment of these eigenvectors makes the calculation of $L'_{\beta\beta}$ extremely easy for all the natural modes. The functions $\underline{J}'_1$ and $\underline{J}''_1$ used here can be identified with $\underline{K}'_{10}$ and $\underline{K}''_{10}$ of [6] respectively. Table II summarizes the results for the electric and magnetic dipole modes of a wire-grid sphere and can be compared with Table I for a solid sphere.

Table II. Wire-grid Sphere

electric dipole mode	magnetic dipole mode
$\lambda'_1(s) = \lambda_1^{o\prime}(s) - s\mu R\delta[1 + c^2/(s^2R^2)]$	$\lambda''_1(s) = \lambda_1^{o\prime\prime} - s\mu R\delta$
$\underline{K}'_1 = \hat{\theta} \sin\theta$	$\underline{K}''_1 = \hat{\phi} \sin\theta$
$s'_{1,\pm1} = -\frac{1}{2}\frac{c}{R}(1-\delta) \pm \frac{i\sqrt{3}}{2}\frac{c}{R}(1+\delta)$	$s''_{1,0} = -\frac{c}{R}(1-\delta)$

Before concluding this section let us summarize the most important result in the language of adding or subtracting impedances to or from the wire-grid model so that it will approximate closer the corresponding closed surface. Since the eigenimpedance Z_β is the negative of the eigenvalue λ_β, (7) can be written as

$$\Delta Z_\beta \equiv Z_\beta(s) - Z_\beta^o(s) = L'_{\beta\beta}(s) \tag{7'}$$

which simply means

(eigenimpedance of wire grid) - (eigenimpedance of closed surface)

$$= L'_{\beta\beta}(s)$$

Although (7) has been obtained by the first-order perturbation theory, in certain cases such as a sphere the result is exact because the unperturbed eigenfunctions also diagonalize the perturbed operator $\underline{\mathcal{L}}'$. For a more general method of calculating $L'_{\beta\beta}$ the reader is referred to [4]. In the case of a sphere, (11) indicates that we should subtract

$$\Delta L = \mu R\delta \quad \text{and} \quad \Delta(1/C_\ell) = \frac{\delta\ell(\ell+1)}{2\epsilon R}$$

from the wire-grid sphere. Notice that $\Delta(1/C_\ell)$ depends on the mode number $\ell(\ell=\beta)$. Thus, the excess series impedance of the wire-grid sphere is given by

$$\Delta Z = s\Delta L + \frac{1}{s}\Delta\left(\frac{1}{C_\ell}\right)$$

for the ℓ-th mode, which is the sum of the ℓ-th electric and the ℓ-th magnetic mode.

SECTION III

DIRECT APPROACH

The $\underline{E}$-field integral equation for a closed surface can take several different forms because the second (capacitive) term, $\underline{E}^{cap}$, in (2) can be manipulated as follows:

$$\underline{E}^{cap} = -\frac{1}{s\varepsilon}\,\hat{n}\times\hat{n}\times\nabla\nabla\cdot\int G(\underline{r},\underline{r}')\underline{K}(\underline{r}')dS' \tag{12a}$$

$$= -\frac{1}{s\varepsilon}\,\hat{n}\times\hat{n}\times\nabla\int G\nabla'\cdot\underline{K}\,dS' \tag{12b}$$

$$= -\frac{1}{s\varepsilon}\,\hat{n}\times\hat{n}\times\int\nabla G\nabla'\cdot\underline{K}\,dS' \tag{12c}$$

$$= -\frac{1}{s\varepsilon}\,\hat{n}\times\hat{n}\times\int G\nabla'\nabla'\cdot\underline{K}\,dS' \tag{12d}$$

$$= -\frac{1}{s\varepsilon}\,\hat{n}\times\hat{n}\times\nabla\int\nabla G\cdot\underline{K}\,dS' \tag{12e}$$

$$= -\frac{1}{s\varepsilon}\,\hat{n}\times\hat{n}\times\int\nabla\nabla G\cdot\underline{K}\,dS' \tag{12f}$$

where we have used $\nabla G = -\nabla' G$ and $\hat{n}\cdot\underline{K} = 0$, and the order of vector multiplications is from right to left. Several remarks are now in order concerning the different forms in expressions (12a)-(12f). Expressions (12c), (12e) and (12f) have to be interpreted as principal-value integrals. Expression (12f) does not exist even in the principal-value sense, but it is widely used in numerical computation because of convenience. To circumvent the difficulty of divergence the so-called extended boundary condition method is introduced in which one only requires the incident field be canceled by the scattered field in an arbitrary region completely within the scatterer, so that $\underline{r}$ and $\underline{r}'$ would never coincide. Expressions (12b), (12c) and (12d) contain derivatives of the unknown and, hence, undesirable from a numerical viewpoint. The matrix elements generated for (12a)-(12f) by, say, some quadrature formulas or the method of moments, are different

and therefore different circuit interpretations will result.

In this section we will evaluate the matrix elements for the $\underline{E}$-field integral equation based on expression (12e), first for a closed surface (Fig. 1a) and then for the corresponding wire-grid model (Fig. 1b). The reasons for choosing expression (12e) as the starting point are implicit in the remarks just made and will also become obvious in the following. Our effort will be spent mostly on the calculations of the diagonal elements and the coupling between neighboring patches or wire segments.

We first divide the closed surface (Fig. 1a) into mathematical patches, say, squares with side a. Then, we limit our attention to the i-th patch which is small compared to the local radii of curvature and, hence, can be treated as a plane square. Let us introduce an arbitrary two-dimensional coordinate system as shown in Fig. 3 and calculate, first, the two terms in the diagonal elements, $\underline{E}_i^{ind}$ and $\underline{E}_i^{cap}$, in the matrix representation of (2). To evaluate $\underline{E}_i^{ind}$ we let the observation point $\underline{r}$ lie at the center $\underline{r}_i$ of the i-th patch, assume the unknown current density to be constant throughout the patch, make low-frequency approximation to the Green's function G (the patch is small compared to wavelengths), and integrate over the i-th patch S_i. Thus,

$$\underline{E}_i^{ind} = s\mu\ \hat{n}_i\times\hat{n}_i\times \int_{S_i} G(\underline{r}_i,\underline{r}')\underline{K}(\underline{r}')dS'$$

$$\simeq \frac{s\mu}{4\pi}\ \hat{n}_i\times\hat{n}_i\times\underline{K}(\underline{r}_i) \int\int \frac{dx'dy'}{\sqrt{(x_i-x')^2+(y_i-y')^2}}$$

$$= \frac{s\mu}{4\pi}\ \hat{n}_i\times(\hat{n}_i\times\underline{K}_i)4 \int_0^{a/2}\int_0^{a/2} \frac{d\xi d\eta}{\sqrt{\xi^2+\eta^2}}$$

$$= \frac{s\mu}{4\pi}\ \hat{n}_i\times(\hat{n}_i\times\underline{K}_i)\ 2a\left[\int_0^1 \ell n\left(1+\sqrt{1+u^2}\right)du+1\right]$$

$$= -\frac{s\mu a}{\pi}\ \ell n(1+\sqrt{2})\underline{K}_i \qquad (13)$$

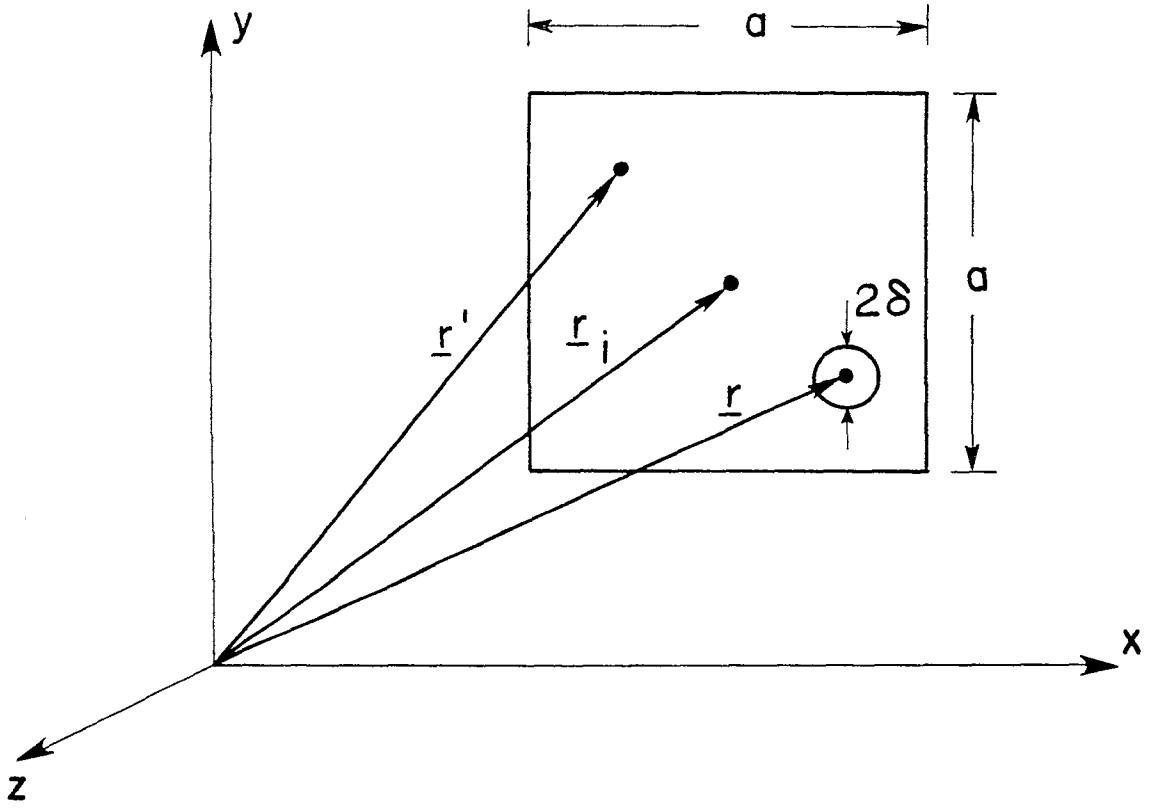

Fig. 3. Coordinates of the i-th square plane patch.

where $\underline{K}_i = \underline{K}(\underline{r}_i)$. Next, we will calculate $\underline{E}_i^{cap}$ given by

$$\underline{E}_i^{cap} = -\frac{1}{s\epsilon}\,\hat{n}_i \times \hat{n}_i \times \left[\nabla \int_{S_i} \nabla G(\underline{r},\underline{r}') \cdot \underline{K}(\underline{r}')\, dS'\right]_{\underline{r}=\underline{r}_i} \tag{14}$$

Before we proceed with the detail of calculation of (14) some preliminary remarks are perhaps necessary. (a) The order of operations as defined in (14) must be strictly followed; otherwise, one will end up with meaningless results. (b) The observation point $\underline{r}$ always lies within the i-th patch. (c) The angular integration over the circle with radius δ (Fig. 3) vanishes as δ tends to zero and , hence, the integral in (14) exists in the principal-value sense. (d) One may, if one wishes, expand the unknown $\underline{K}$ in a Taylor series about $\underline{r}_i$ and keep more than one term in the series. But physical intuition tells us that $\underline{K}$ is practically constant over a small patch and there is no need to keep terms beyond the first one in the series unless the coefficient in the first term happens to be zero. After some simple vector algebra, (14) gives, in terms of the local coordinate system of Fig. 3,

$$\underline{E}_i^{cap} = \hat{x}\, I_x + \hat{y}\, I_y \tag{15}$$

where

$$I_x = -\frac{1}{4\pi s\epsilon}\left[\frac{\partial}{\partial x}\int_{S_i}\left\{\frac{x-x'}{R^3}\,K_x(x',y') + \frac{y-y'}{R^3}\,K_y(x',y')\right\} dx'dy'\right]_{\substack{x=x_i \\ y=y_i}}$$

$$I_y = -\frac{1}{4\pi s\epsilon}\left[\frac{\partial}{\partial y}\int_{S_i}\left\{\frac{x-x'}{R^3}\,K_x(x',y') + \frac{y-y'}{R^3}\,K_y(x',y')\right\} dx'dy'\right]_{\substack{x=x_i \\ y=y_i}}$$

$$R = \sqrt{(x-x')^2 + (y-y')^2} \tag{16}$$

Then, keeping only the first term in the Taylor series expansion of $\underline{K}$, we have

$$I_x = -\frac{1}{4\pi s\varepsilon}\left[\frac{\partial}{\partial x}\int_{y-y_i+a/2}^{y-y_i-a/2}\int_{x-x_i+a/2}^{x-x_i-a/2}\left\{\frac{\xi}{(\xi^2+\eta^2)^{3/2}}K_x(x_i,y_i) + \frac{\eta}{(\xi^2+\eta^2)^{3/2}}K_y(x_i,y_i)\right\}d\xi d\eta\right]_{\substack{x=x_i\\ y=y_i}}$$

$$= -\frac{1}{4\pi s\varepsilon}\,2a\,K_x\int_0^{a/2}\frac{d\eta}{[\eta^2+(a/2)^2]^{3/2}} = -\frac{\sqrt{2}}{\pi s\varepsilon a}K_x(\underline{r}_i) \tag{17}$$

Similarly, we have

$$I_y = -\frac{\sqrt{2}}{\pi s\varepsilon a}K_y(\underline{r}_i)$$

Substitution into (15) gives, with $\underline{K}_i = \underline{K}(\underline{r}_i)$,

$$\underline{E}_i^{cap} = -\frac{\sqrt{2}}{\pi s\varepsilon a}\underline{K}_i \tag{18}$$

Collecting the results from (13) and (18) we have

$$L_{ii} = -\frac{s\mu a}{\pi}\ell n(1+\sqrt{2}) - \frac{\sqrt{2}}{\pi s\varepsilon a} \tag{19}$$

to be the diagonal matrix elements of the $\underline{E}$-field integral equation,

$$\underline{\underline{\mathcal{L}}}_o \cdot \underline{K} = -\underline{E}_{tan}^{inc},$$

over the closed surface of a perfectly conducting surface. Let us rewrite (19) in a more general form:

$$L_{ii} = -sL_i - \frac{1}{sC_i} \tag{20}$$

with

$$L_i = \frac{\ell n(1+\sqrt{2})}{4\pi} \mu p_i \simeq 0.07\ \mu p_i \qquad \text{henries}$$

$$C_i = \frac{\pi}{4\sqrt{2}} \varepsilon p_i \simeq 0.56\ \varepsilon p_i \qquad \text{farads}$$

p_i = perimeter of the i-th zone

We now turn to the calculation of the diagonal elements of the wire-grid model using the so-called thin-wire approximation in which the integrals in (12c), (12e) and (12f) all exist because $\underline{r}$ and $\underline{r}'$ never coincide. Then, expressions (12e) and (12f) are equivalent and either can be used for the evaluation of matrix elements. Let us consider the i-th segment of the wire grid and a is small compared to wavelengths (Fig. 4). Then, the diagonal matrix element L^w_{ii} of (2) for the wire grid is given by

$$L^w_{ii}\ I_i = -\frac{s\mu}{4\pi} \int_{y_i-a/2}^{y_i+a/2} \frac{I(y')dy'}{\sqrt{(y_i-y')^2+r_o^2}} + \frac{1}{4\pi s\varepsilon} \int_{y_i-a/2}^{y_i+a/2} \frac{\partial^2}{\partial y_i^2} \frac{I(y')dy'}{\sqrt{(y_i-y')^2+r_o^2}}$$

$$= -\left(\frac{s\mu a\Omega}{4\pi} + \frac{2}{s\varepsilon a\pi}\right)\frac{I_i}{a} \qquad (21)$$

where I has been assumed constant over a segment, $I_i = I(y_i)$, $\Omega = 2\ \ell n(a/r_o)$, and I_i/a should be identified with the y-component of the surface current density $\underline{K}_i$ of the corresponding closed surface.

So far the calculation has been limited to the diagonal matrix elements for the actual body and its wire-grid model. The mutual interaction between neighboring patches and between the corresponding wire segments can be calculated with similar techniques. The tacit assumptions in these calculations are that the region under consideration is small in terms of wavelengths and that it can be approximated by a planar surface. Fig. 5 shows the patches and wires for which the results are obtained and presented in Table III.

Starting with the diagonal elements we now make some comments concerning the results shown in Table III. For $\Omega = 6$ (i.e., $a \simeq 20\ r_o$), which is about the value used in most wire-grid computer codes, $\Omega/4 = 1.5$ while $\ell n(1+\sqrt{2}) \simeq 0.881$, the difference being about a factor of 1.7. For the capacitive diagonal term the

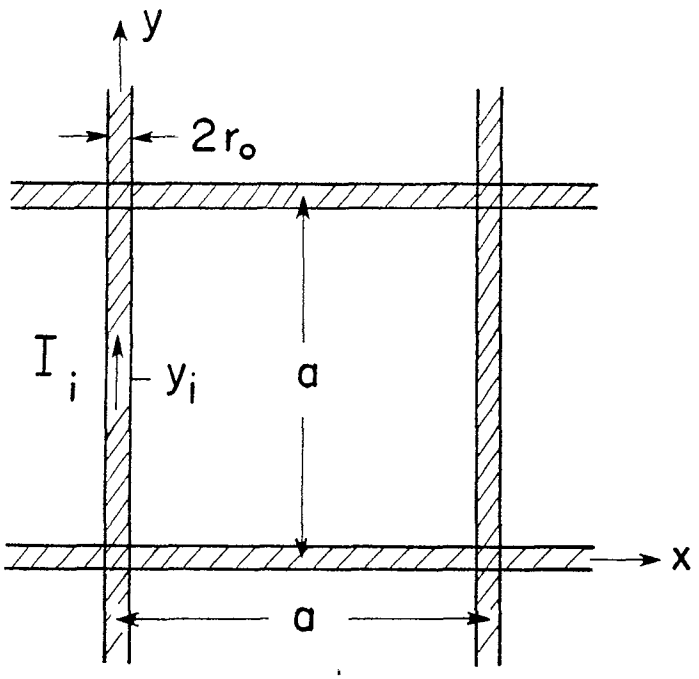

Fig. 4. The i-th segment of the wire-grid model.

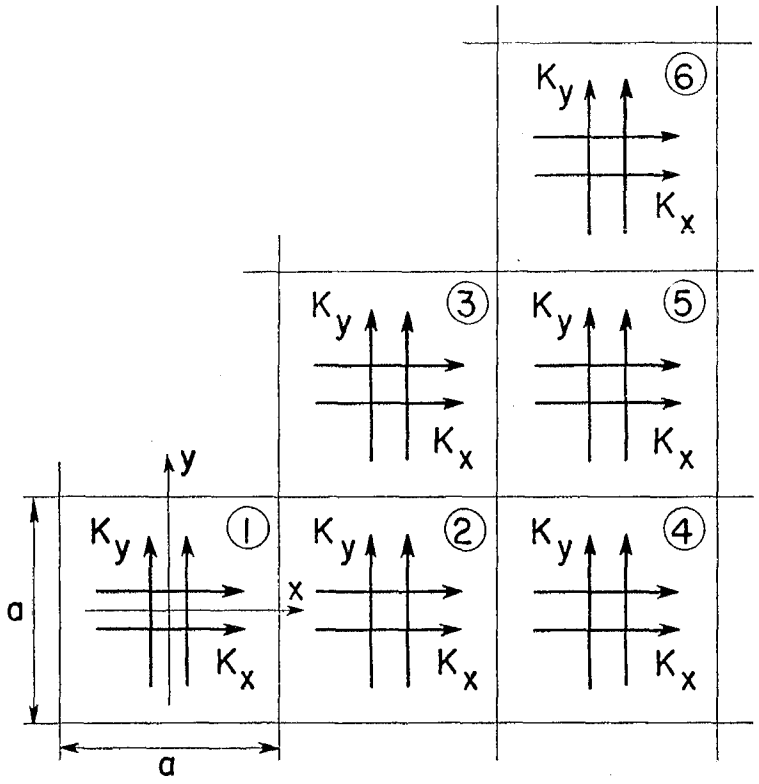

Fig. 5a. Current definition and patch numbers used in Table IIIa.

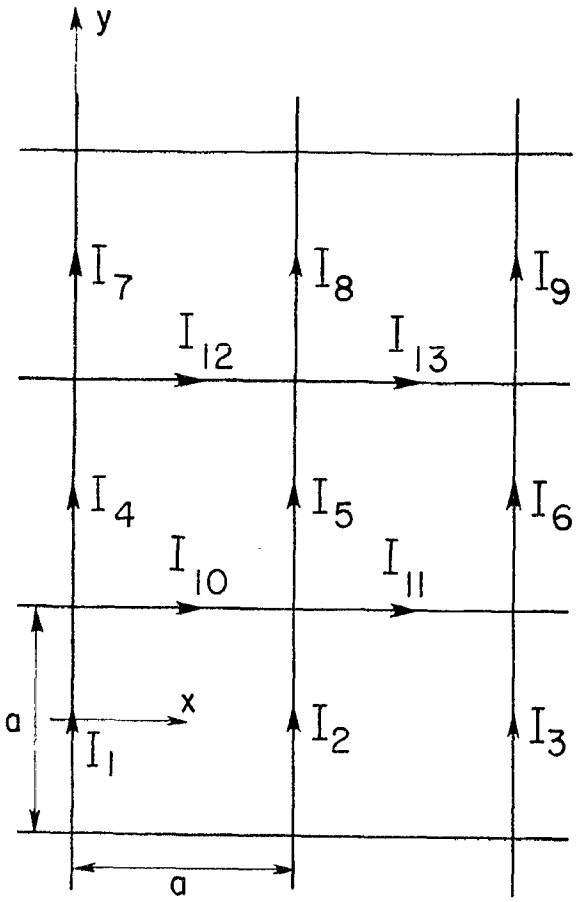

Fig. 5b. Definition of wire currents used in Table IIIb.

Table IIIa. Matrix elements from the $\underline{E}$-field integral equation for the patches of Fig. 5a.

	Patch #1		Patch #2		Patch #3	
	K_x	K_y	K_x	K_y	K_x	K_y
$E_x^{cap}(0,0)s\varepsilon a$	-0.4502	0	0.1915	0	-0.0177	0.0494
$E_y^{cap}(0,0)s\varepsilon a$	0	-0.4502	0	-0.0769	0.0494	-0.0177
$E_x^{ind}(0,0)/s\mu a$	-0.2805	0	0.0826	0	0.0577	0
$E_y^{ind}(0,0)/s\mu a$	0	-0.2805	0	0.0826	0	0.0577

	Patch #4		Patch #5		Patch #6	
	K_x	K_y	K_x	K_y	K_x	K_y
$E_x^{cap}(0,0)s\varepsilon a$	0.0211	0	0.0106	0.0089	0.0018	0.0054
$E_y^{cap}(0,0)s\varepsilon a$	0	-0.0102	0.0089	-0.0029	0.0054	0.0018
$E_x^{ind}(0,0)/s\mu a$	0.0402	0	0.0359	0	0.0283	0
$E_y^{ind}(0,0)/s\mu a$	0	0.0402	0	0.0359	0	0.0283

Example: The current density $\underline{K}_3 = K_{3x}\,\hat{x} + K_{3y}\,\hat{y}$ on patch #3 gives the following tangential electric field at the center of patch #1,

$$\underline{E}_{tan}^{sc}(0,0) = \left(0.0577\, s\mu a\, K_x - \frac{0.0177}{s\varepsilon a} K_x + \frac{0.0494}{s\varepsilon a} K_y\right)\hat{x}$$

$$+\left(\frac{0.0494}{s\varepsilon a} K_x - \frac{0.0177}{s\varepsilon a} K_y\right)\hat{y}$$

Table IIIb. Matrix elements from the E-field integral equation for the wire segments of Fig. 5b.

	I_1	I_2	I_3	I_4	I_5	I_6
$E_y^{cap}(0,0)s\varepsilon a$	$-2/\pi$	-0.0712	-0.0091	0.2829	-0.0081	-0.0031
$E_y^{ind}(0,0)/s\mu a$	$-\Omega/4\pi$	0.0766	0.0394	-0.0874	0.0568	0.0355

	I_7	I_8	I_9	I_{10}	I_{11}	I_{12}	I_{13}
$E_y^{cap}(0,0)s\varepsilon a$	0.0226	0.0102	0.0016	-0.2892	-0.0239	-0.0150	-0.0127
$E_y^{ind}(0,0)/s\mu a$	0.0406	0.0360	0.0282	0	0	0	0

Example: The current $\underline{I}_3 = I_3 \hat{y}$ on wire segment #3 gives the following axial electric field at the center of wire segment #1,

$$E_y^{sc}(0,0) = \left(0.0394\ s\mu a - \frac{0.0091}{s\varepsilon a}\right)\frac{I_3}{a}$$

the difference is about 41%. We also note that both the inductive and capacitive terms of the diagonal elements of the wire-grid model are larger than the corresponding elements of the actual (patch) case. This result is intuitively clear since a wire segment has a larger impedance than does the corresponding patch. Therefore, the wire-grid model underestimates the EMP-induced currents on the actual structure.

Turning to the off-diagonal elements in Table III we see that the inductive parts of the matrix elements with respect to immediate neighbors agree within 8% in the two cases. For more distant patches and wire segments the difference is less than 1%. The capacitive terms, however, differ more than the inductive terms in the two cases, as can be seen from Table III. The difference (in the capacitive terms) will be reduced to less than 3% for more distant patches and wire segments than those presented in the table. We mention in passing that the interaction between distant patches and wire segments outside the range covered by Table III can be accounted for using a dipole approximation of the patches and wires.

Since each patch (wire segment) is small in terms of wavelengths so that $|sa/c| << 1$, the capacitive term of each matrix element increases as the patch (wire) size decreases. This rather perturbing behavior can be attributed to the fact that the $\underline{E}$-field equation is not an integral equation but an integro-differential equation. Therefore, this is an inherent property of the $\underline{E}$-field equation and will occur in solving this equation numerically using the so-called method of moments regardless of the base functions (piece-wise linear, piece-wise sinusoidal, etc.) that one may use. This behavior of the elements makes the matrix ill-conditioned and it is not clear that the numerical solution converges as the patch size decreases (matrix size increases).

SECTION IV

CIRCUIT APPROACH

In the preceding section we saw how the diagonal matrix elements and the matrix elements connecting neighboring patches or wire segments were generated starting with expression (12e) for the capacitive term. In a straightforward but messy manner one can calculate all the matrix elements for N patches on a closed surface or $2N$ wire segments of the corresponding grid model. In so doing one will end up with a $2N \times 2N$ matrix. In the language of circuit theory one then has a $2N$-port network, the lumped elements of which are given by the matrix elements and are interconnected in a highly complex manner. In this section we will derive a much simpler circuit representation of the wire grid and calculate the circuit elements in the representation. We then argue that the same representation holds approximately also for the closed surface at least locally and calculate the circuit elements by integration over patches. The derivation of the circuit representation is mostly heuristic, intermingled with physical arguments and simple mathematical operations.

When one looks at the wire grid as shown in Fig. 1b, one sees a self-inductance and a self-capacitance for each wire segment (which is assumed to be electrically short) and mutual inductances and capacitances between neighboring segments. If each wire segment is thin enough (i.e., $\Omega = 2 \ell n(a/r_o) \geq 10$), the mutual inductances and capacitances can be neglected in comparison to the self-inductance and self-capacitance whose values are given by

$$L_w = \frac{\mu a \Omega}{4\pi}, \qquad C_w = \frac{4\pi\epsilon a}{\Omega} \tag{22}$$

When the wire segments are of the same length a and radius r_o, the self-capacitance, C, of each wire cross (which is one basic unit of the grid model) is simply $2C_w$. Thus, one arrives at the circuit representation of Fig. 6, which may be termed a "two-dimensional" transmission-line model of a wire grid. It must be borne in mind, however, that such a representation is valid only when the grid is planar and radiation losses are neglected.

To see how Fig. 6 comes about we start with expression (12a) for the

capacitive term in the $\underline{E}$-field integral equation. The integral equation now takes the form, with $s = j\omega$,

$$j\omega\mu\,\hat{n}\times\hat{n}\times\int G\,\underline{J}\,dS' - \frac{1}{j\omega\varepsilon}\,\hat{n}\times\hat{n}\times\nabla\nabla\cdot\int G\,\underline{J}\,dS' = -\underline{E}^{inc}_{tan} \tag{23}$$

Because of the presence of $\nabla\nabla$ outside the integral sign the branch current in one wire segment will be related to the currents in neighboring segments through the shunt currents flowing into the capacitances, in a way similar to the usual one-dimensional transmission line. The values for L_w and C_w given by (22) can be obtained from (23) by noting that G is highly peaked at $\underline{r}' = \underline{r}$ and hence the integral in (23) over, say, the i-th segment gives approximately

$$\int_{S_i} G(\underline{r}_i,\underline{r}')\underline{J}(\underline{r}')dS' \simeq \underline{J}(\underline{r}_i)\int_{S_i} G(\underline{r}_i,\underline{r}')dS' \simeq \frac{\Omega r_o}{2}\,\underline{J}(\underline{r}_i) \tag{24}$$

where $\underline{r}_i$ is the midpoint of the i-th segment. The differential operator $\nabla\nabla$ in the second term of (23) must now be interpreted as $\nabla_i\nabla_i$; that is to say, $\nabla_i\nabla_i\cdot\underline{J}(\underline{r}_i)$ means taking the difference of the values of $\underline{J}$ evaluated at the centers of neighboring segments. With these considerations we arrive at the circuit representation Fig. 6 with radiation losses neglected.

For the corresponding closed surface (Fig. 1a) we assume that locally the circuit representation is the same as Fig. 6 except that the inductance and capacitance values will be different. The difference stems from the evaluation of (24) over a square of side a rather than along a wire segment of length a and radius r_o. Over the i-th patch we then have

$$\int_{S_i} G(\underline{r}_i,\underline{r}')\underline{K}(\underline{r}')dS' \simeq \underline{K}(\underline{r}_i)\int_{S_i} G(\underline{r}_i,\underline{r}')dS' = \frac{a\,\ell n(1+\sqrt{2})}{\pi}\,\underline{K}(\underline{r}_i) \tag{25}$$

where we have used (13) to evaluate the integral.

To sum up, the inductance L and capacitance C in the circuit representation Fig. 6 are given in Table IV.

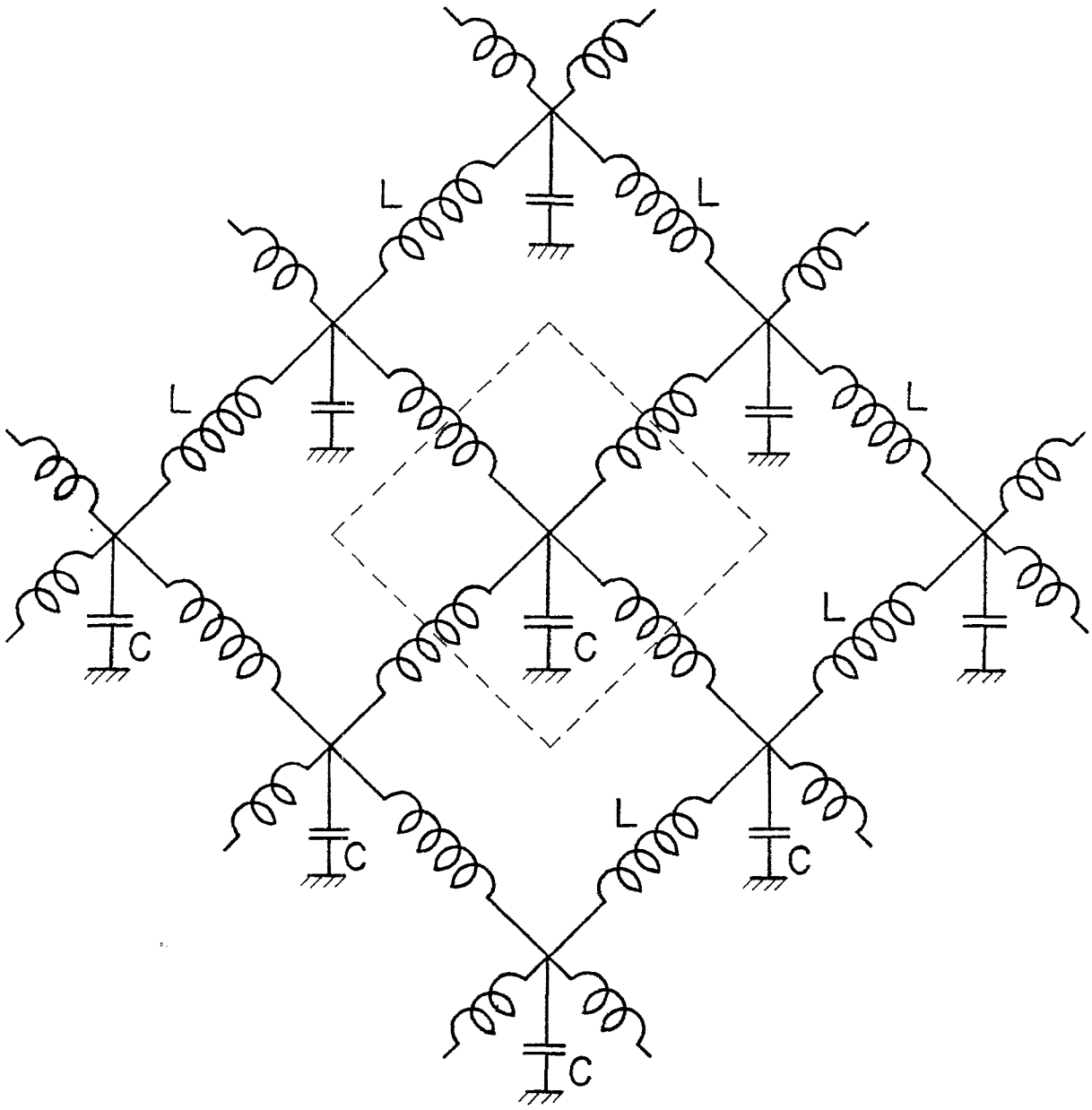

Fig. 6. Local circuit representation of the wire-grid model shown in Fig. 1b.

Table IV. Values of L and C in Fig. 6

	closed surface	wire grid
L	$\frac{\mu a \ln(1+\sqrt{2})}{\pi}$	$\frac{\mu a \Omega}{4\pi}$
C	$\frac{\pi \varepsilon a}{\ln(1+\sqrt{2})}$	$\frac{8\pi \varepsilon a}{\Omega}$

Notice that the inductance value of the closed surface in Table IV is the same as the self-inductance calculated in Section III. However, the self-capacitance values are different because the capacitance in Table IV is a shunt capacitance with respect to infinity, whereas the self-capacitance value in Section III is referred to a series capacitance.

There are two further points about Table IV that need to be discussed. First, the capacitance value for each wire cross of the wire-grid model can be split into two parallel capacitances, each having a value $4\pi\varepsilon a/\Omega$. In so doing the propagation speed along either direction of the grid is given by $1/\sqrt{\mu\varepsilon}$, as it should. The second and perhaps most important point is that the difference in inductance ΔL and the difference in capacitance ΔC between the closed surface and its wire-grid model can be calculated from Table IV and expressed in a more recognizable form. To do this we include one more term in the asymptotic formula (22) for the inductance L_w. As expected, this term turns out to be a constant, i.e., independent of the wire radius. Without going into the details of the derivation we merely give the result:

$$L_w = \frac{\mu a}{4\pi}\left[\Omega - 2\ln(e/2)\right] + O\left(\frac{1}{\Omega}\right)$$

$$= \frac{\mu a}{2\pi}\ln\left(\frac{a}{2\pi r_o}\right) + \frac{\mu a \ln(4\pi/e)}{2\pi} + O\left(\frac{1}{\Omega}\right) \tag{26}$$

Thus, we have

$$\Delta L = L_{\text{wire grid}} - L_{\text{closed surface}}$$

$$= \frac{\mu a}{2\pi} \ell n\left(\frac{a}{2\pi r_o}\right) + \frac{\mu a \ell n(4\pi/e)}{2\pi} - \frac{\mu a \ell n(1+\sqrt{2})}{\pi} + 0\left(\frac{1}{\Omega}\right)$$

$$= \frac{\mu a}{2\pi} \ell n\left(\frac{a}{2\pi r_o}\right) + 0.244\ \mu a - 0.281\ \mu a + 0\left(\frac{1}{\Omega}\right)$$

$$\simeq \frac{\mu a}{2\pi} \ell n\left(\frac{a}{2\pi r_o}\right) \qquad (27)$$

This result is in agreement with that of Reference 7 where the effect of replacing conducting plates with wires for parallel-plate EMP simulators is discussed. Expression (27) is obtained with the assumption that

$$\frac{1}{2\pi} \ell n\left(\frac{a}{2\pi r_o}\right) >> 0.04$$

which certainly is compatible with the thin-wire approximation. For the difference in capacitance we simply have

$$\Delta C = C_{\text{wire grid}} - C_{\text{closed surface}}$$

$$= -\frac{\pi}{\ell n(1+\sqrt{2})} \varepsilon a + \frac{8\pi}{\Omega} \varepsilon a$$

$$= -3.56\ \varepsilon a + 0\left(\frac{1}{\Omega}\right) \qquad (28)$$

Expressions (27) and (28) mean that the wire grid has more inductance but less capacitance than does the corresponding closed surface, as one would have expected.

ACKNOWLEDGMENT

We are grateful to Dr. Carl Baum for his generous suggestions and constructive comments throughout the work.

REFERENCES

[1] Castillo, J. P., K. C. Chen and B. K. Singaraju, "Calculation of Currents Induced on a Disk by a Wire Grid Code," Interaction Note 230, 14 February 1975.

[2] Kontorovich, M. I., "Averaged Boundary Conditions at the Surface of a Grating With Square Mesh," Rad. Eng. Electron. Phys., Vol.8, No.9, 1963, pp.1446-1454.

[3] Schiff, L. I., Quantum Mechanics, McGraw-Hill, New York, 1955.

[4] Baum, C. E., "On the Eigenmode Expansion Method for Electromagnetic Scattering and Antenna Problems, Part I: Some Basic Relations for Eigenmode Expansions and Their Relation to the Singularity Expansion," Interaction Note 229, 13 January 1975.

[5] Marin, L., "Natural-Mode Representation of Transient Scattering From Rotationally Symmetric Perfectly Conducting Bodies and Numerical Results for a Prolate Spheroid," Interaction Notes, Note 119, Sept. 1972.

[6] Lee, K. S. H., and L. Marin, "Interaction of External System-Generated EMP With Space Systems," Theoretical Notes, Note 179, August 1973. See also "A Charged Particle Moving Near a Perfectly Conducting Sphere," IEEE Trans. Antennas Propagat., Vol.AP-22, No.5, Sept. 1974.

[7] Baum, C. E., "Impedances and Field Distributions for Parallel Plate Transmission Line Simulators," Sensor and Simulation Notes, Note 21, June 1966.